The Dynamics of Functional Brain Networks: Integrated Network States during Cognitive Task Performance

Highlights

- The human brain network traverses segregated and integrated states over time

- Integrated states enable fast, effective performance on an N-back task

- Integrated states track with fluctuations in pupil diameter

- Cognitive performance relates to the dynamic reorganization of brain architecture

Authors

James M. Shine, Patrick G. Bissett, Peter T. Bell, ..., Krzysztof J. Gorgolewski, Craig A. Moodie, Russell A. Poldrack

Correspondence

macshine@stanford.edu

In Brief

Shine et al. use dynamic analyses of fMRI data to demonstrate that the network architecture of the human brain fluctuates between states of high and low global integration that track with effective task performance and may relate to fluctuations in arousal.

Neuron

Article

CellPress

The Dynamics of Functional Brain Networks: Integrated Network States during Cognitive Task Performance

James M. Shine,[1,2,6,*] Patrick G. Bissett,[1] Peter T. Bell,[3] Oluwasanmi Koyejo,[1,5] Joshua H. Balsters,[4] Krzysztof J. Gorgolewski,[1] Craig A. Moodie,[1] and Russell A. Poldrack[1]

[1]Department of Psychology, Stanford University, Stanford, CA 94305, USA
[2]Neuroscience Research Australia, University of New South Wales, Sydney NSW 2052, Australia
[3]University of Queensland Centre for Clinical Research, University of Queensland, Brisbane QLD 4072, Australia
[4]Department of Health Sciences and Technology, Neural Control of Movement Laboratory, ETH Zurich, 8092 Zurich, Switzerland
[5]Present address: Department of Computer Science, University of Illinois, Urbana-Champaign, IL 60606, USA
[6]Lead Contact
*Correspondence: macshine@stanford.edu
http://dx.doi.org/10.1016/j.neuron.2016.09.018

SUMMARY

Higher brain function relies upon the ability to flexibly integrate information across specialized communities of brain regions; however, it is unclear how this mechanism manifests over time. In this study, we used time-resolved network analysis of fMRI data to demonstrate that the human brain traverses between functional states that maximize either segregation into tight-knit communities or integration across otherwise disparate neural regions. Integrated states enable faster and more accurate performance on a cognitive task, and are associated with dilations in pupil diameter, suggesting that ascending neuromodulatory systems may govern the transition between these alternative modes of brain function. Together, our results confirm a direct link between cognitive performance and the dynamic reorganization of the network structure of the brain.

INTRODUCTION

Within the brain, a highly dynamic functional landscape unfolds on a relatively fixed structural scaffold (Deco et al., 2015; Shen et al., 2015) in which the emergence of momentary neural coalitions forms the basis for complex cognitive functions (Bassett et al., 2015; Cole et al., 2014), learning (Bassett et al., 2011), and consciousness (Barttfeld et al., 2015; Godwin et al., 2015). This view of brain function highlights the role of individual brain regions within the context of a broader neural network (Bullmore and Sporns, 2012). Others have noted the importance of time-sensitive descriptions of brain activity in understanding the functional relevance of alterations in this network structure under different behavioral conditions (Varela et al., 2001).

Time-resolved analyses of functional neuroimaging data provide a unique opportunity to examine these time-varying reconfigurations in global network structure. These experiments provide a sensitive method for non-invasively identifying time-sensitive shifts in inter-areal synchrony, which has been proposed as a key mechanism for effective communication between distant neural regions (Fries, 2015; Varela et al., 2001). To this end, recent experiments using fMRI data have demonstrated that global brain signals transition between states of high and low connectivity strength over time (Zalesky et al., 2014) and that these fluctuations are related to coordinated patterns of network topology (Betzel et al., 2016); however, the psychological relevance of these fluctuations in network topology remains poorly understood.

In the present work, we show that dynamic fluctuations in network structure relate to ongoing cognitive function, and further demonstrate a relation between these fluctuations and integration within a network of frontoparietal, striatal, and thalamic regions that track with the ascending neuromodulatory system of the brain, as characterized using pupillometry (Joshi et al., 2016). Together, the results of our experiments provide mechanistic evidence to support the role of global network integration in effective cognitive performance.

RESULTS

Fluctuations in Network Cartography

To elucidate fluctuations in the network structure of the brain over time, we computed a windowed estimate of functional connectivity (Shine et al., 2015) from a cohort of 92 unrelated subjects obtained from the Human Connectome Project (HCP; see Experimental Procedures; Smith et al., 2013). After identifying the community structure of the brain's functional connectivity network (Rubinov and Sporns, 2010), we estimated the importance of each region for maintaining this evolving network structure by calculating its connectivity both within (W_T) and between (B_T) each community (see Experimental Procedures; Guimerà and Nunes Amaral, 2005; Sporns and Betzel, 2016). While previous studies have clustered these metrics at the regional level using pre-defined cartographic boundaries (Guimerà and Nunes Amaral, 2005; Mattar et al., 2015), we hypothesized that the brain should fluctuate as a whole between cartographic extremes that were characterized by either segregation (i.e., the extent
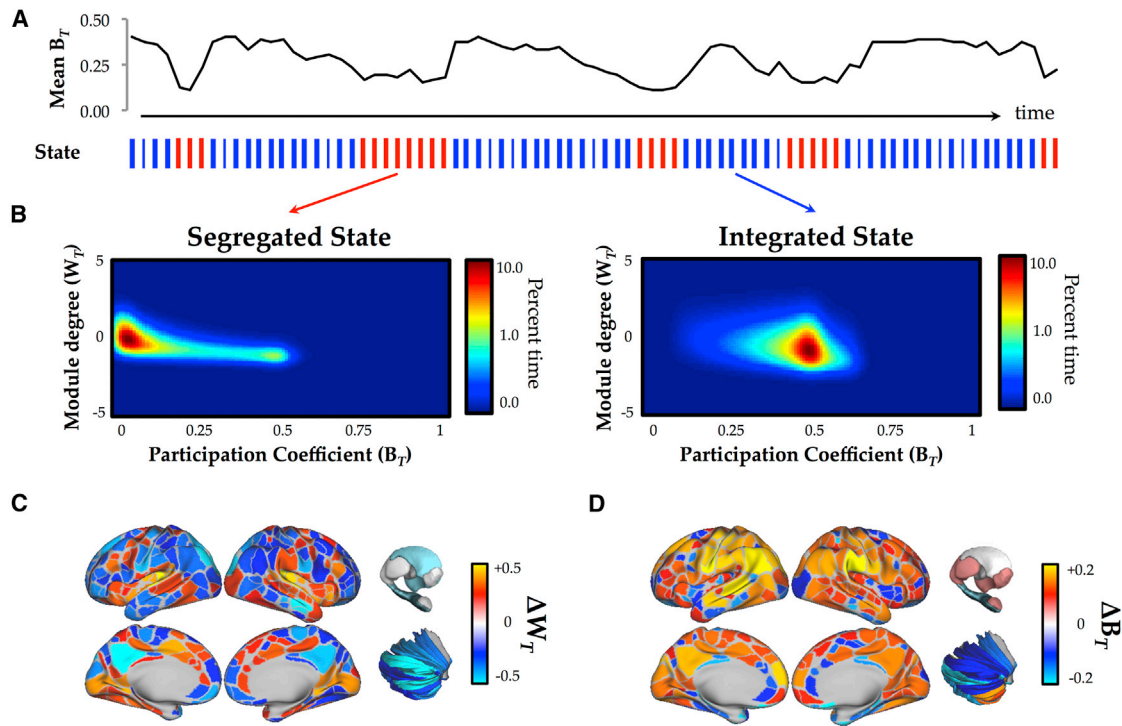
Figure 1. Dynamic Fluctuations in Cartography
(A) Upper: a representative time series of the mean B_T for a single individual from the Discovery cohort (HCP #100307). Lower: each temporal window was partitioned into one of two topological "states" using *k*-means clustering (red, segregated; blue, integrated).
(B) The mean cartographic profile of both the segregated and integrated states (HCP Discovery cohort; n = 92).
(C) Regions with greater W_T in the integrated than segregated state.
(D) Regions with greater B_T in the integrated than segregated state.

to which communication occurs primarily within tight-knit communities of regions) or integration (i.e., the extent of communication between distinct regions; Deco et al., 2015), which might otherwise be obscured by reduction into classes defined by these arbitrary cartographic boundaries.

To test this hypothesis in the resting state, we created a novel analysis technique to assess the temporal classification into two states without requiring the grouping of each region into a pre-defined cartographic class (Guimerà and Nunes Amaral, 2005), which we refer to here as the "cartographic profile." Subject-level *k*-means clustering of these full profiles across time (*k* = 2, with stable clustering at higher values of *k*; see Experimental Procedures; Figure S1, available online) identified modes of information processing that were characterized by either integration or segregation (Figure 1A). The resting brain explored a dynamical repertoire within this topological regime (greater than expected by a stationary null model), fluctuating aperiodically between the integrated and segregated temporal states, with the majority of time spent in integrated states (70.32% ± 1.4% of rest session; all variability measures reported as SDs). Although the majority of the group-level fluctuations occurred in inter-modular connectivity (i.e., B_T values transitioned between high and low states en masse), we also observed window-to-window fluctuations in intra-modular connectivity (W_T) within individual parcels (see Video 1 at https://github.

com/macshine/coupling for a demonstration of the fluctuations of the cartographic profile over time).

The two states also showed differential patterns of regional inter-modular connectivity (Figures 1C and 2C), with the integrated states characterized by a global increase in inter-modular communication across the brain (false discovery rate [FDR] $\alpha < 0.05$ for all 375 individual parcels). This was also reflected in graph-theoretic measures of network-wide integration: temporal windows associated with segregated states had significantly elevated modularity ($Q_S = 0.55 \pm 0.1$ versus $Q_I = 0.42 \pm 0.2$; Cohen's d = 0.9; p = 10^{-11}; Sporns and Betzel, 2016), whereas those associated with the integrated states had greater global efficiency ($E_S = 0.18 \pm 0.03$ versus $E_I = 0.24 \pm 0.05$; d = 1.5; p = 10^{-8}; Bullmore and Sporns, 2012). The shift toward integration was most prominent in sensory and attentional networks (Figure 1D; FDR $\alpha < 0.05$), whereas segregated states were associated with relatively higher participation within regions in the default mode network, suggesting that the cartographic profile may reflect changes in the engagement of attention and cognition over time (Corbetta and Shulman, 2002). Importantly, the fluctuations in global network topology occurred independently of the mean framewise displacement in each temporal frame (TR) (mean r = 0.01 ± 0.01), nuisance signals from cerebrospinal fluid (CSF) and deep cerebral white matter (WM) (mean r = −0.02 ± 0.01),
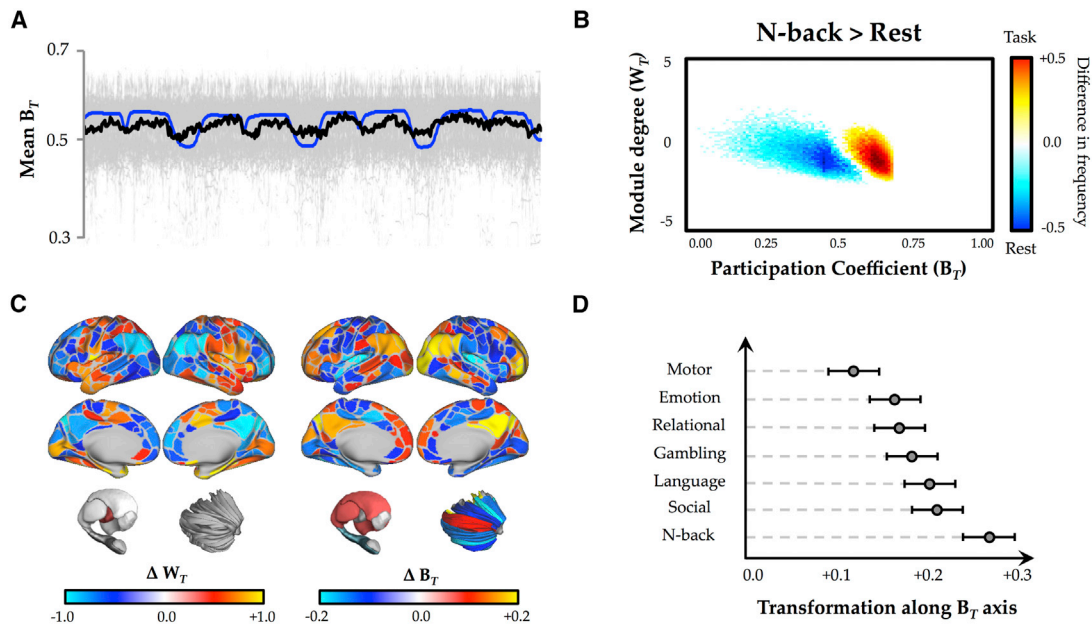
Figure 2. Alteration of Cartographic Profile during Task Performance

(A) Time series plot demonstrating the close temporal relationship between mean B_T across 100 subjects (thick black line; individual subject data plotted in gray) and task-block regressors (blue line) (Pearson's correlation between regressor and group mean B_T, r = 0.521).

(B) Regions of the 2D joint histogram that were significantly different between N-back task blocks and the resting state (paired-samples t test). Colored points indicate regions that survived false discovery correction (FDR $\alpha < 0.05$): red/yellow, increased frequency during N-back task blocks; blue/light blue, increased frequency during resting state (FDR $\alpha < 0.05$).

(C) Surface projections of parcels associated with higher W_T (left) or B_T (right) during the N-back task, when compared the resting state: frontoparietal and subcortical "hub" regions showed elevated B_T during task, whereas W_T was elevated in primary systems and decreased in default mode regions.

(D) A plot quantifying the extent to which the cartographic profile shifted toward integration in the six tasks in the HCP dataset in comparison to the resting state along the between-module axis (error bars reflect SD across the Discovery cohort).

and number of modules estimated within each temporal window (mean r = 0.03 ± 0.10).

Task-Based Alterations in the Cartographic Profile

We next examined whether the balance between network integration and segregation tracked with ongoing cognitive function using data from a cognitively demanding "N-back" task (Barch et al., 2013). We observed a strong correlation between fluctuations in cartography across all parcels and the blocks of the experimental task (group mean Pearson's r = 0.521; R^2 = 0.27; p = 10^{-10}; Figure 2A; Video 2, https://github.com/macshine/coupling), as well as a distinct alteration in the cartographic profile when compared to the resting state (Figure 2B). These changes were coincident with increased task-driven connectivity between frontoparietal, dorsal attention, cingulo-opercular, and visual networks (2-back versus 0-back blocks; FDR q < 0.05; Figure S4), suggesting that global integration may have facilitated communication between otherwise segregated systems during the more challenging 2-back condition. Importantly, the extent of integration remained correlated with the task regressor even after controlling for the global signal (mean r = 0.452 ± 0.21; p = 10^{-10}) and the mean time-resolved connectivity across all parcels (mean r = 0.393 ± 0.14; p = 10^{-9}), suggesting that the fluctuations in topology were not simply driven by constraints imposed by the task structure.

Together, these results suggest that the brain transitions into a state of higher global integration in order to meet extrinsic task demands. Indeed, all of the 375 regions showed a significant shift toward greater inter-modular connectivity (B_T) during the N-back task when compared to the resting state (FDR $\alpha < 0.05$ for all 375 regions). Despite this global shift toward integration, the effect was most pronounced within frontoparietal, default mode, striatal, and thalamic regions (Figure 2C), many of which have been previously identified as belonging to a "rich club" of densely interconnected, high-degree "hub" nodes that are critical for the resilience and stability of the global brain network (van den Heuvel and Sporns, 2013). Importantly, the involvement of these highly interconnected hub regions during the task would likely facilitate effective communication between specialist regions that would otherwise remain isolated, thus affording a larger repertoire of potential responses to deal with the challenges of the task.

To determine whether network topology was sensitive to specific task demands, we calculated the cartographic profile in the remaining six tasks from the HCP in the same cohort of 92 subjects (Barch et al., 2013). While the performance of each task also led to an increase in global integration relative to rest, the effect was less pronounced than the lateral shift observed in the N-back task, particularly when compared to the relatively simple motor task (88.8% of parcels showed higher B_T in the
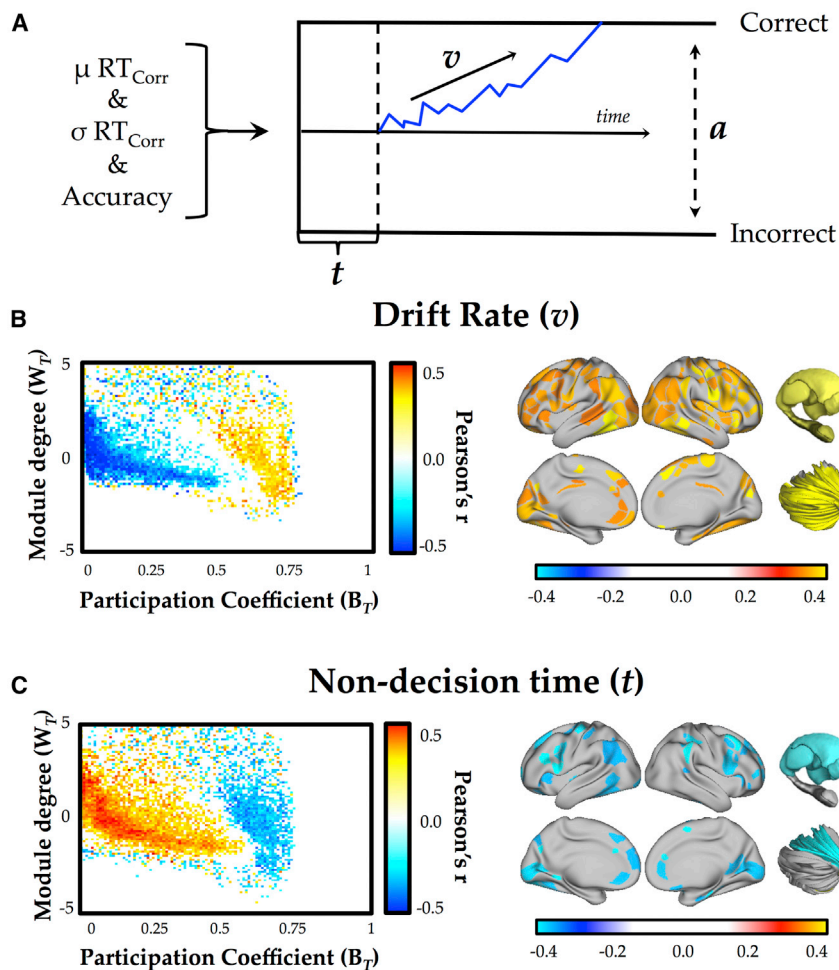
A

B

Drift Rate (*v*)

Figure 3. Relationship between Task Performance and the Cartographic Profile

(A) A graphical depiction of the drift-diffusion model, which uses the mean and SD of a subject's reaction time and performance accuracy to estimate the "drift rate," or rate of evidence accumulation (*v*), the length of non-decision time (*t*), and the response boundary (*a*).

(B) Left: group-level correlation between drift rate on the N-back task and each bin of the mean cartographic profile during the N-back task in the Discovery cohort. Right: parcels showing a positive correlation between mean B_T and drift rate.

(C) Left: group-level correlation between non-decision time on the N-back task and each bin of the mean cartographic profile during the N-back task in the Discovery cohort. Right: parcels showing a negative correlation between mean B_T and non-decision time (FDR α = 0.05). No bins of the cartographic profile showed a consistent response with the response boundary. Similarly, no parcels showed a significant correlation between W_T and any of the three diffusion model fits.

C

Non-decision time (*t*)

behavior (response time distributions and accuracy) on the more cognitively challenging 2-back trials within the N-back task using the EZ-diffusion model (Wagenmakers et al., 2007; Figure 3A). The diffusion model provides a decomposition of behavioral performance into cognitively relevant latent variables representing the speed and accuracy of information processing (drift rate, "*v*"), the speed of perceptual and motor processes not directly related to the decision pro-

N-back task; FDR α < 0.05). This effect was quantified by estimating the affine transformation required to align each subject's resting cartographic profile with their profile during each task (transformation along the B_T axis relative to rest; Figure 2D). These results demonstrate that the extent of reconfiguration varies as a function of task: the relatively simple motor task, which involved repetitive movements of specific effectors, was associated with greatest segregation, whereas the more complex N-back task, which required complex working memory updating and cognitive control, was associated with greatest integration. The other five tasks recruited levels of integration between these two extremes. Together, these results suggest that integration may be particularly important for more difficult tasks, perhaps involving cognitive control; however, additional work will be necessary to identify the specific demands that drive global integration.

Investigating the Relationship between Cartography and Behavior

Based on these findings, we predicted that a more globally integrated network architecture would give rise to faster, more effective information processing during task performance. To test this hypothesis, we fit a drift diffusion model to each subject's

cess (non-decision time, "*t*"), and a flexible measure of response caution (boundary separation, "*a*"; Ratcliff, 1978). Theoretically, faster progression throughout all stages of information processing from perception through action should be reflected in a positive relationship between global integration and both faster drift rate and shorter non-decision time, whereas integration should be independent of the boundary parameter.

We compared these model parameters to the mean N-back cartographic profile across the Discovery cohort (Figure 3A). The extent of global network integration in the cartographic profile was positively correlated with drift rate (Figure 3B), inversely correlated with non-decision time (Figure 3C), and had no relationship to the boundary threshold. Each of these patterns was replicated in a separate cohort of 92 subjects. For both drift rate and non-decision time (and in both the Discovery and Replication cohorts), the relationship between cognitive function and integration was most pronounced across frontoparietal, striatal, thalamic, and pallidal regions (FDR α < 0.05; Figures 3B and 3C). Together, these results suggest that a globally efficient, integrated network architecture supports fast, effective computation throughout the cognitive processing stream (Krienen et al., 2014), potentially through the facilitation of parallel processing mechanisms (Sigman and Dehaene, 2008).
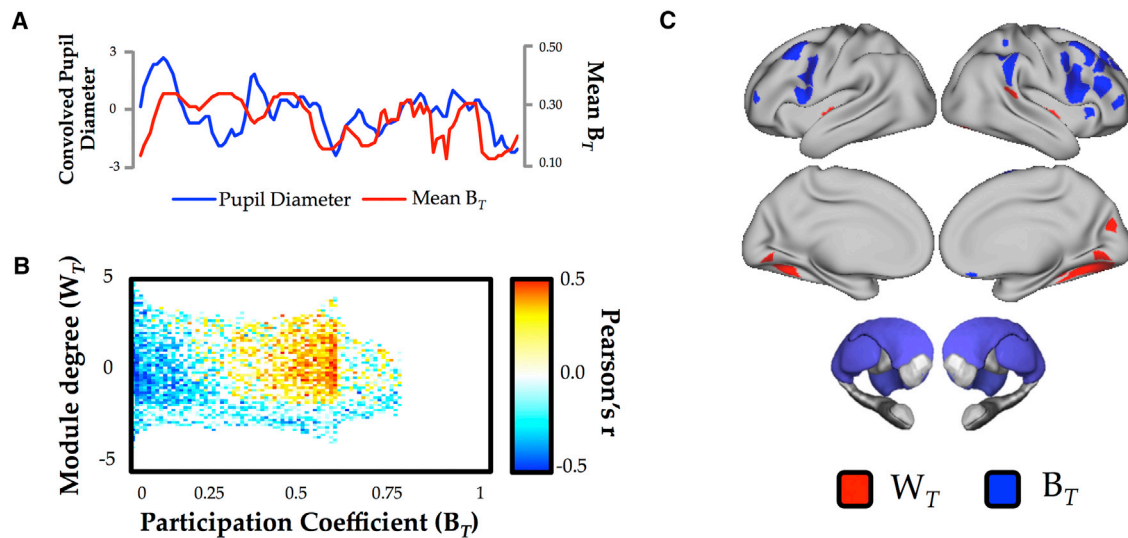
Figure 4. Relationship between Cartography and Pupillometry

(A) An example time series (subject #1) showing the covariance between the pupil diameter (after convolution with a hemodynamic response function; blue) and mean between-module connectivity (B_T; red).

(B) Mean Pearson correlation between each bin of the cartographic profile and the convolved pupil diameter. Across the cohort of 14 subjects, we observed a positive relationship between pupil diameter and network-level integration (FDR α = 0.05).

(C) Results from a conjunction analysis (FDR $\alpha < 0.05$) that compared relationships between W_T (red) or B_T (blue) and drift rate (positive correlation), non-decision time (inverse correlation), and pupillometry (positive correlation). There were no cerebellar parcels above threshold in all three contrasts.

Network Cartography Fluctuates with Pupil Diameter

Based on the results of these experiments, we hypothesized that neuromodulatory brain systems that mediate neural gain control (Aston-Jones and Cohen, 2005) may play an important role in regulating global integration. Recent invasive electrophysiological recordings in non-human primates have shown that non-luminance-related fluctuations in pupil diameter track with neural firing in ascending neuromodulatory systems, such as the locus coeruleus, confirming the well-established proposal (Kahneman, 1973) that pupil diameter is a surrogate measure for arousal and task engagement (McGinley et al., 2015). Therefore, we measured pupil diameter from individuals in a separate resting state dataset (14 individuals; TR = 2 s; 3.5mm^3 voxels; 204 volumes; Murphy et al., 2014) and compared alterations in pupil diameter with the cartographic profile (w = 10 TRs). As predicted, we observed a positive correlation between pupil diameter and mean B_T (group mean r = 0.241 ± 0.06; R^2 = 0.06; p = 10^{-5}; Figure 4) that was maximal within frontoparietal, striatal, and thalamic regions. In keeping with Eldar et al. (2013), these results suggest that the observed global fluctuations in network structure over time may have been driven by ongoing dynamic alterations in ascending neuromodulatory input to the cortex and subcortex, which, through the modulation of neural gain, may have mediated increases in connectivity between otherwise segregated regions of the brain.

Identifying Regions Related to Global Integration

To further investigate the neurobiological mechanisms responsible for fluctuations in network topology over time, we used a parcel-wise conjunction analysis (Nichols et al., 2005) to identify a set of regions that were significantly related to drift rate, non-decision time, and pupil diameter. This analysis revealed a right-lateralized network of frontal, parietal, thalamic, and striatal regions that were associated with consistently elevated B_T across the three comparisons (blue; Figure 4C) and a set of regions in visual cortex and insula that were associated with elevated W_T (red; Figure 4C). Together, these results highlight a distributed network of brain regions that mediate the computational integration required for effective cognitive processing.

Reproducibility

To test the reproducibility of our results, we performed three separate replication analyses: (1) on a second resting state session from the same cohort of 92 unrelated subjects, (2) on a different cohort of 92 unrelated subjects from the HCP consortium, and (3) on 152 subjects from a separate dataset acquired at a different scanning site, using high-resolution functional data from the NKI Rockland dataset (Nooner et al., 2012). For each analysis in the resting state, we replicated the analyses described above and then summarized each outcome measure of interest at the group level (minimum r = 0.564; all p < 0.001; see Experimental Procedures). In the task data, each of the relationships identified between the cartographic profile and behavior was replicated in the second set of 92 individuals from the HCP (both r > 0.610; p < 0.001; Figure S2). These results suggest that the time-resolved measures identified in this study were reliable across sessions, individuals, and independent datasets collected using different scanners and imaging protocols.

DISCUSSION

In this manuscript, we mapped the spatiotemporal dynamics of complex network structure in the human brain, revealing a

dynamical system that fluctuates between segregated and integrated network topology (Figure 1). The cartographic profile observed in the resting state was modulated by the performance of a range of cognitive tasks in proportion to task demands (Figure 2). Importantly, the extent to which the brain was globally integrated was correlated with faster drift rate and shorter non-decision time during the N-back task, suggesting that integration relates to fast and effective cognitive performance (Figure 3). We then showed that integration within the functional connectome correlated with increases in pupil diameter (Figure 4), highlighting a potential neurobiological mechanism responsible for modulating network-level dynamics in the human brain. Finally, we were able to demonstrate that a network of right-lateralized frontoparietal, striatal, and thalamic regions was responsible for mediating the effects of integration on cognitive function (Figure 4C).

In our final experiment, we demonstrated that the fluctuations in network cartography in the resting state correlate with changes in pupil diameter (Figure 4), which itself is a marker of arousal and behavioral engagement (McGinley et al., 2015). The locus coeruleus (Aston-Jones and Cohen, 2005) is known to modulate pupil diameter (Joshi et al., 2016), and thus, by inference, may play a role in the modulation of fluctuations in global network topology through phasic alterations in neural gain (Eldar et al., 2013). Thus, our results extend previous studies that have demonstrated a crucial link between neural gain and functional connectivity (Eldar et al., 2013; Yellin et al., 2015; van den Brink et al., 2016) by showing that fluctuations in neural gain are linked to alterations in network topology that, in turn, relate to effective behavioral performance.

There is a wealth of evidence to suggest that neuromodulatory inputs can have complex, non-linear effects on network organization and behavior (Bargmann and Marder, 2013), perhaps as a result of the balance between the "top-down" attentional modulation of network architecture (Sara, 2009) and "bottom-up" neuromodulatory input from the brainstem (Safaai et al., 2015). The network of right-lateralized cortical regions consistently associated with elevations in integration in our study provides further support for this hypothesis (Figure 4C), as ascending noradrenergic inputs preferentially impact neural function within the right cortical hemisphere (Pearlson and Robinson, 1981). While our results suggest a crucial role for ascending noradrenergic gain control, the topological organization of the functional connectome is likely to arise as the end result of multiple competing factors, including changes in tone within other neuromodulatory systems, such as the basal cholinergic nuclei (Steriade and McCarley, 2013); local interactions among functional regions; and activity in other diffuse projection systems, such as the intralaminar thalamic nuclei (Van der Werf et al., 2002).

Irrespective of the precise mechanism driving global fluctuations, our results suggest that system-wide alterations in network topology facilitate more effective behavioral performance, a hypothesis that has already garnered support from studies both in network dynamics (Kitzbichler et al., 2011) and pupillometry (Murphy et al., 2016). There is now growing evidence to support the notion that the brain traverses a metastable state-space in time (Deco et al., 2015), balancing the opposing tendencies for specialized, segregated processing with the

need for global coordination and integration (Tognoli and Kelso, 2014). In addition, others have recently shown that fluctuations in network topology relate to distinct patterns of behavior during cognitive tasks (Alavash et al., 2016; Vatansever et al., 2015). Here, we extend these studies by demonstrating fluctuations in network topology that relate to computationally meaningful measures of effective behavioral performance.

Although we were able to demonstrate that greater system-wide integration was associated with improved cognitive performance on an N-back task, the precise role of network topology in cognition requires further exploration. The N-back task is often used as a measure of cognitive control, which itself is a complex construct composed of dissociable sub-components, such as updating, set-shifting, and response inhibition (Miyake et al., 2000), that likely rely on overlapping, yet distinct, neural architectures (Duncan, 2010; Poldrack et al., 2011). We demonstrated that the extent of reconfiguration varies as a function of task: the relatively simple motor task, which involved repetitive movements of specific effectors, was associated with greatest segregation, whereas the more complex cognitive N-back task, which required complex working memory updating and cognitive control, was associated with greatest integration. The other five tasks recruited levels of integration between these two extremes (see Figure 2D). Together, these results suggest that integration may be particularly important for more difficult tasks, perhaps involving cognitive control; however, additional work will be necessary to identify the specific cognitive demands that drive global integration.

There are also some important limitations to note in our study. First, although we provide indirect evidence for the relationship between neural gain and effective cognitive performance, the direct relationship between ascending neuromodulatory input to the brain and network topology requires further confirmation, perhaps utilizing the temporal resolution afforded by electrophysiological measures or the direct investigation of the influence of major neurotransmitter systems using neuromodulatory techniques, such as optogenetics. Second, on the basis of fMRI data alone, it is not possible to determine whether global integration facilitated increased connectivity between otherwise disparate regions, or whether the topological changes were merely a necessary byproduct of increased communication between specialist regions of the brain (Ramsey et al., 2010). Although the resolution of this question would likely require the causal manipulation of the brain (Keller et al., 2014), the utilization of computational modeling approaches may offer some insight into the underlying mechanism (Deco et al., 2015). Finally, although we directly compared the Multiplication of Temporal Derivatives (MTD) approach to sliding-window Pearson's correlation, the standard approach used to calculate time-resolved connectivity, there are many techniques used to estimate these measures (Hutchison et al., 2013), and as such, further work is required to determine the robustness of the fluctuations in network topology across multiple time-sensitive connectivity metrics.

Together, our results demonstrate that global brain integration is closely related to cognitive function during an N-back task. By catalyzing communication between specialist regions of the brain that would otherwise remain segregated, global integration increases an individual's ability to accomplish complex

CellPress

cognitive tasks, potentially accelerating behavioral innovation and improving fitness in novel scenarios (Shanahan, 2012). As such, global integration is an important candidate mechanism responsible for the evolution of complex brain networks (van den Heuvel et al., 2016) and, hence, for explaining the mechanism through which the brain creates complex, adaptive behavior.

EXPERIMENTAL PROCEDURES

Data Acquisition

For the primary discovery analysis, minimally preprocessed resting fMRI data were acquired from 100 unrelated participants from the HCP (mean age 29.5 years, 55% female; Glasser et al., 2013). For each participant, 14 min, 30 s of resting state data were acquired using multiband gradient-echo EPI (echo planar imaging). The following parameters were used for data acquisition: TR = 720 ms, echo time = 33.1 ms, multiband factor = 8, flip angle = 52°, field of view = 208 × 180 mm (matrix = 104 × 90), 2 × 2 × 2 isotropic voxels with 72 slices, alternated LR/RL phase encoding.

In addition to the discovery analysis, we also performed an extensive series of replication analyses, including (1) data from the same participants using resting state data acquired during a second rest scan during the same scanning session, (2) an independent cohort of 100 unrelated participants from the HCP dataset using identical acquisition parameters at the same scanning site, and (3) an out-of-sample replication using data collected from the NKI Rockland sample (TR = 650 ms; voxel size 3 mm³) as part of the 1000 Functional Connectomes Project (Nooner et al., 2012). The data reported in this paper were made publicly available by the HCP and 1000 Functional Connectomes project and were subject to their own institutional review board requirements.

Data Preprocessing

Bias field correction and motion correction (12 linear degrees of freedom [DOFs] using FSL's FLIRT) were applied to the HCP resting state data as part of the minimal preprocessing pipeline (Glasser et al., 2013). The first 100 time points were discarded from the data due to the presence of an evoked auditory signal associated with noise in the scanner. Resting state data acquired from the NKI Rockland sample were realigned to correct for head motion, and then each participant's functional scans were registered to both their T1-weighted structural image and then to the MNI152 atlas using FSL boundary-based registration and Advanced Normalization Tools software (Avants et al., 2008). After co-registration, data were manually inspected and of the 173 original participants, 11 (6.3%) scans were discarded due to insufficient coverage of orbitofrontal cortex, temporopolar cortex, and/or cerebellum.

Temporal artifacts were identified in each dataset by calculating framewise displacement (FD) from the derivatives of the six rigid-body realignment parameters estimated during standard volume realignment (Power et al., 2014), as well as the root-mean-square change in BOLD signal from volume to volume (DVARS). Frames associated with FD >0.5 mm or DVARS >5% were identified, and participants with greater than 20% of the resting time points exceeding these values were excluded from further analysis (HCP group 1, 8/100; HCP group 2, 8/100; NKI group, 10/162). Due to concerns associated with the alteration of the temporal structure of the images, the data used in the main analysis were not "scrubbed" (Power et al., 2014); however, we did compare the results of our experiment with scrubbed data (missing values corrected using interpolation) and found strong correspondence between the outcome measures of the two studies (see Validation). Following artifact detection, nuisance covariates associated with the twelve linear head movement parameters (and their temporal derivatives), FD, DVARS, and anatomical masks from the CSF and deep cerebral WM were regressed from the data using the CompCor strategy (Behzadi et al., 2007). Finally, in keeping with previous time-resolved connectivity experiments (Bassett et al., 2015), a temporal band pass filter (0.071 < f < 0.125 Hz) was applied to the data (see Validation).

Brain Parcellation

Following preprocessing, the mean time series was extracted from 375 pre-defined regions of interest (ROIs). To ensure whole-brain coverage, we extracted 333 cortical parcels (161 and 162 regions from the left and right hemispheres, respectively) using the Gordon atlas (Gordon et al., 2016), 14 subcortical regions from Harvard-Oxford subcortical atlas (bilateral thalamus, caudate, putamen, ventral striatum, globus pallidus, amygdala, and hippocampus), and 28 cerebellar regions from the SUIT atlas (Diedrichsen et al., 2009). These ROIs were chosen to maximize our ability to interrogate fluctuations in network architecture over time; however, it bears mention that functional divisions may differ across subjects (Laumann et al., 2015).

Time-Resolved Functional Connectivity

To estimate functional connectivity between the 375 ROIs, we used a recently described statistical technique (MTD; Shine et al., 2015) that allows greater temporal resolution of time-resolved connectivity in BOLD time series data when compared to the conventional sliding-window Pearson's correlation coefficient (Shine et al., 2015). The MTD is computed by calculating the point-wise product of temporal derivative of pairwise time series (Equation 1). The MTD is averaged over a temporal window, w, in order to reduce the contamination of high-frequency noise in the time-resolved connectivity data. Code is freely available at https://github.com/macshine/coupling/.

$$MTD_{ijt} = \frac{1}{w} \sum_{t}^{t+w} \frac{(dt_{it} \times dt_{jt})}{(\sigma_{dt_i} \times \sigma_{dt_j})} \qquad \text{(Equation 1)}$$

Equation 1 shows the MTD, where for each time point, t, the MTD for the pairwise interaction between region i and j is defined according to Equation 1, where dt is the first temporal derivative of the ith or jth time series at time t, σ is the SD of the temporal derivative time series for region i or j, and w is the window length of the simple moving average. This equation can then be calculated over the course of a time series to obtain an estimate of time-resolved connectivity between pairs of regions.

Time-resolved functional connectivity was calculated between all 375 brain regions using the MTD (Shine et al., 2015) within a sliding temporal window of 14 time points (10.1 s for HCP; 16 time points for NKI data, ~10.4 s). Individual functional connectivity matrices were calculated within each temporal window, thus generating an unthresholded (i.e., signed and weighted) 3D adjacency matrix (region × region × time) for each participant. Previous work has shown that when using the MTD, a window length of seven time points provides optimal sensitivity and specificity for detecting dynamic changes in functional connectivity structure in simulated time series data (Shine et al., 2015). To balance these benefits with the need to track changes in slow cortical fluctuations that are hypothesized to fluctuate at ~0.1 Hz (Shen et al., 2015), we used a temporal window of 14 time points to calculate a simple moving average of the MTD, which allowed for estimates of signals at approximately 0.1 Hz. While there are statistical arguments to suggest that the potential effects of noise can render estimation of connectivity matrices difficult with smaller samples, it is currently unclear whether these issues will have the same effects on the covariance estimates created with the MTD. However, we note that the MTD is more sensitive to changes in covariance than connectivity (Shine et al., 2015), and others have shown that covariance is a more reliable marker of coupling strength in BOLD data (Cole et al., 2016). Most importantly, as we show, our analyses were reliable and replicable using the MTD across multiple datasets.

Time-Resolved Community Structure

The Louvain modularity algorithm from the Brain Connectivity Toolbox (BCT; Rubinov and Sporns, 2010) was used in combination with the MTD to estimate both time-averaged and time-resolved community structure. The Louvain algorithm iteratively maximizes the modularity statistic, Q, for different community assignments until the maximum possible score of Q has been obtained (see Equation 2). The modularity estimate for a given network is therefore a quantification of the extent to which the network may be subdivided into communities with stronger within-module than between-module connections.

$$Q_T = \frac{1}{\nu^+} \sum_{ij} \left(w_{ij}^+ - e_{ij}^+ \right) \delta_{M_i M_j} - \frac{1}{\nu^+ + \nu^-} \sum_{ij} \left(w_{ij}^- - e_{ij}^- \right) \delta_{M_i M_j} \qquad \text{(Equation 2)}$$

Equation 2 shows the Louvain modularity algorithm, where v is the total weight of the network (sum of all negative and positive connections), w_{ij} is the weighted and signed connection between regions i and j, e_{ij} is the strength of a connection divided by the total weight of the network, and δ_{MiMj} is set to 1 when regions are in the same community and 0 otherwise. "+" and "−" superscripts denote all positive and negative connections, respectively.

For each temporal window, the community assignment for each region was assessed 500 times and a consensus partition was identified using a fine-tuning algorithm from the BCT (http://www.brain-connectivity-toolbox.net/). This afforded an estimate of both the time-resolved modularity (Q_T) and cluster assignment (Ci_T) within each temporal window for each participant in the study. All graph theoretical measures were calculated on weighted and signed connectivity matrices (Rubinov and Sporns, 2010), and the γ parameter was set to 1.

Based on time-resolved community assignments, we estimated within-module connectivity by calculating the time-resolved module-degree Z score (W_T, within-module strength) for each region in our analysis (Equation 3; Guimerà and Nunes Amaral, 2005).

$$W_{iT} = \frac{\kappa_{iT} - \overline{\kappa}_{s_i T}}{\sigma_{\kappa_{s_i T}}} \qquad \text{(Equation 3)}$$

Equation 3 shows the module-degree Z score, W_{iT}, where κ_{iT} is the strength of the connections of region i to other regions in its module s_i at time T, $\overline{\kappa}_{s_i T}$ is the average of κ over all the regions in s_i at time T, and $\sigma_{\kappa_{s_i T}}$ is the SD of κ in s_i at time T.

Time-Resolved Hub Structure

The participation coefficient, B_T, quantifies the extent to which a region connects across all modules (i.e., between-module strength) and has previously been used to successfully characterize hubs within brain networks (e.g., see Power et al., 2013). The B_T for each region was calculated within each temporal window using Equation 4.

$$B_{iT} = 1 - \sum_{s=1}^{n_M} \left(\frac{\kappa_{isT}}{\kappa_{iT}} \right)^2 \qquad \text{(Equation 4)}$$

Equation 4 shows the participation coefficient B_{iT}, where κ_{isT} is the strength of the positive connections of region i to regions in module s at time T, and κ_{iT} is the sum of strengths of all positive connections of region i at time T. The participation coefficient of a region is therefore close to 1 if its connections are uniformly distributed among all the modules and 0 if all of its links are within its own module.

Cartographic Profiling

To track fluctuations in cartography over time, we created a novel analysis technique that did not require the labeling of each node into a pre-defined cartographic class (Guimerà and Nunes Amaral, 2005). For each temporal window, we computed a joint histogram of within- and between-module connectivity measures, which we refer to here as a "cartographic profile" (Figure 1). Code for this analysis is freely available at https://github.com/macshine/integration/. To test whether the cartographic profile of the resting brain fluctuated over time between two topological extremes, we performed clustering of temporal windows without the use of cartographic class labels. To do so, we classified the joint histogram of each temporal window (which is naive to cartographic boundaries) over time using a k-means clustering analysis ($k = 2$). As a result of this analysis, each window was assigned to one of two clusters. k-means was repeated with 500 random restarts to mitigate the sensitivity of k-means to initial conditions.

To ensure that the a priori choice of two clusters for the k-means analysis was reflective of the broader patterns in the data across multiple values of k, we re-ran the clustering analysis in the discovery cohort of 92 subjects across a range of k values (2–20) and then compared the resultant cluster partitions to the $k = 2$ clusters by calculating the mutual information between each pair of partitions. The partition identified at each value of k was strongly similar to the pattern identified at $k = 2$ (mean mutual information = 0.400 ± 0.02; Figure S1). We also provided further evidence for this partition by performing a principle component analysis for each subject's data—this test demonstrated that the first two principle components for each subject were associated with the integrated (20.2% ± 1.4% variance) or segregated state (4.9% ± 2.3% variance).

To explicitly test whether the resting brain fluctuated more frequently than a stationary null model, we calculated the absolute value of the window-to-window difference in the mean B_T score for each iteration of a vector autoregression (VAR) null model. In keeping with Zalesky et al. (2014), VAR model order was set at 11, appropriately mimicking the expected temporal signature of the BOLD response in 0.72 s TR data. The mean covariance matrix across all 92 subjects from the discovery group was used to generate 2,500 independent null datasets, which allows for the appropriate estimation of the tails of non-parametric distributions (Nichols and Holmes, 2002). These time series were then filtered in a similar fashion to the BOLD data. For each analysis, the maximum statistic was concatenated for each independent simulation. We then calculated the 95th percentile of this distribution and used this value to determine whether the resting state data fluctuated more frequently than the null model. In the discovery cohort, 16.1% ± 1.1% of temporal windows were associated with deviations $\geq$ 95th percentile of the VAR null model (i.e., greater than the predicted 5%), suggesting that the resting state was associated with significant dynamic fluctuations in topology. Importantly, the significant fluctuations along the B_T axis remained after correcting for ongoing changes in the number of modules per temporal window.

To estimate patterns of topology associated with each state, the original 3D connectivity matrix containing MTD values was then reorganized into those windows associated with the two states (defined in the k-means analysis; $k = 2$). The modularity of these windows associated with each of the two states was then compared statistically using an independent-samples t test. Importantly, the two states were matched on graph density, suggesting that the fluctuations in B_T did not occur simply due to alterations in network sparsity over time. A similar technique was used to estimate the global efficiency of each temporal window. As global efficiency (Equation 5) cannot be computed from networks with negative weights (Barch et al., 2013), we first thresholded the connectivity matrix within each window to include only positive edge weights before calculating global efficiency on the remaining connected component.

$$E_{glob} = \frac{2}{n(n-1)} \sum_{i < j \in G}^{n} \frac{1}{d_{i,j}} \qquad \text{(Equation 5)}$$

Equation 5 shows the global efficiency of a network, where n denotes the total nodes in the network and $d_{i,j}$ denotes the shortest path between a node i and neighboring node j.

To estimate the patterns of brain connectivity associated with each state, we binned each region's W_T and B_T scores into those windows associated with either integrated or segregated states (using the $k = 2$ partition). We then compared the regional W_T and B_T scores across the two states using an independent-samples t test. As expected, all 375 parcels demonstrated higher B_T in the more integrated states, whereas none of the 375 parcels showed significantly different W_T in either state (FDR $\alpha < 0.05$). For interpretation and display, regional B_T scores were converted into Z scores and then projected onto surface renderings (Figure 1). We also performed a targeted analysis to determine whether activity and connectivity within the default network were related to fluctuations in B_T (activity, group mean r = −0.044 ± 0.09, p = 10^{-5}; connectivity, group mean r = 0.127 ± 0.09, p = 10^{-12}).

Task-Based Alterations in the Cartographic Profile

To assess task-based functional connectivity, preprocessed data from the original 92 unrelated subjects from the discovery cohort were collected while these subjects performed seven different tasks in the fMRI (see Barch et al., 2013 for further details of each experimental paradigm). The mean time series was then extracted from the same 375 regions as defined in the resting state analysis. To control for spurious patterns of connectivity associated with task-evoked activity, we first regressed the hemodynamic response function

CellPress

(HRF)-convolved task block data from each time series. The MTD metric was then calculated on the residuals of this regression using a window length of 14 TRs (~10 s at 0.72 s TR). These data were then subjected to a cartographic profiling analysis in a similar fashion to the resting state data. We also directly modeled the mean time-resolved network-level connectivity associated with 2-back and 0-back blocks in the N-back task using a mixed-effects general linear model (FDR q < 0.05; Figure S4). The network membership of each of the parcels was defined according to a previous study (Gordon et al., 2016).

To compare the patterns of time-resolved connectivity across the N-back task to those observed during rest, we tested whether any bins within the 2D cartographic profile were significantly modulated by task by running a mixed-effects general linear model analysis at the individual level, fitting the group-averaged joint histogram to regressors tracking 2-back, 0-back, and rest blocks in both the motor and the N-back task, separately. We then compared the task blocks and the resting state data statistically using separate two-sided, one-sample t tests across subjects (FDR α < 0.05). We observed a rightward deviation in the mean cartographic profile during the 2-back versus 0-back block; however, to allow direct comparison across tasks and rest, we opted to include the mean 2-back profile for each comparison described in the main manuscript. A similar analysis was run comparing the mean W_T and B_T across all 375 parcels. As in previous steps, the regional B_T scores were converted into Z scores (otherwise, the regional heterogeneity associated with each task would be hidden within the much larger mean effect) and then projected onto surface renderings (Figure 2).

In order to assess the alteration in the cartographic profile as a function of task performance, we estimated the affine transformation (using a correlation cost function with $3°$ of freedom, including translation and rotation parameters) between each individual subject's resting state cartographic profile and the profile observed in each of the seven tasks. To ensure that any differences observed during task performance were not confounded by fluctuations in global signal or connectivity, we replicated the analysis after separately regressing the global signal and the mean MTD value across all parcels (global signal, mean r = 0.452 ± 0.21, p = 10^{-10}; mean MTD, mean r = 0.393 ± 0.14, p = 10^{-9}).

Investigating the Relationship between Cartography and Behavior

To interrogate the relationship between the cartographic profile and behavioral performance, we fit an EZ-diffusion model to the performance measures from the N-back task (Wagenmakers et al., 2007). This model takes in the mean response time (RT) on correct trials, mean variance of RT across correct trials, and mean accuracy across the task and computes from them a value for drift rate, boundary separation, and non-decision time—the three main parameters for the diffusion model (Figure 3). We used the EZ-diffusion model instead of alternative diffusion fitting routines (e.g., fast-dm or DMAT) because previous work has shown that the EZ-diffusion model is particularly effective for recovering individual differences in parameter values, which were of particular interest in this experiment (van Ravenzwaaij and Oberauer, 2009). After fitting each subject's data to the diffusion model, we then performed a group-level Pearson's correlation between each bin of the mean joint histogram in each task and the three outcome measures associated with the N-back task: the drift rate (Figure 3B), the non-decision time (Figure 3C), and the boundary threshold (data not shown, as no bins survived multiple comparisons correction). The model was fit on results from the 2-back task blocks, as a many subjects made no errors on the 0-back condition, thus precluding our ability to fit their data to the parameters of the drift diffusion model. For each comparison, the null hypothesis of no relationship was rejected after FDR correction (p < 0.05). We also compared the cartographic profile with median reaction time and accuracy for both the cohorts and observed a similar relationship between integration and improved performance.

Some work suggests that the EZ-diffusion model performs poorly when there are "contaminants" in the data (Ratcliff et al., 2015), which are trials in which the usual diffusion parameters do not apply (like fast guesses and attentional lapses). We searched for evidence of contaminants in our data and found no evidence of them (i.e., the few fast responses [110 RTs <400 ms across both samples] were not guesses [93% accuracy was the same as

the 93% accuracy for all trials]). Therefore, we proceeded with the EZ-diffusion model, which performs as well as or better than more complicated fitting routines when contaminants are not present (Ratcliff et al., 2015; van Ravenzwaaij and Oberauer, 2009).

Network Cartography Fluctuates with Pupil Diameter

To test the hypothesis that fluctuations in cartography related to activity in ascending neuromodulatory systems, we acquired a separate dataset of 14 individuals (mean age 29 years, 8/14 male) in which pupil diameter was measured over time during the quiet resting state (TR = 2 s; 3.5 mm^3 voxels; 204 volumes; Murphy et al., 2014). Participants were instructed to relax, think of nothing in particular, and maintain fixation for 8 min at a centrally presented crosshair (subtending 0.65° of the visual angle). BOLD fMRI data were preprocessed using SPM8 software (www.fil.ion.ucl.ac.uk/spm). Pupil diameter was recorded continuously from the left eye at rest and during task using an iView X MRI-SV eye tracker (SMI) at a sampling rate of 60 Hz. Pupillometric data were thoroughly preprocessed to remove potential sources of noise (see Murphy et al., 2014 for details) and then downsampled to a 0.5 Hz sampling rate (in order to match the sampling frequency of the fMRI data). A pupil diameter vector for each scanning run was then convolved with the informed basis set to yield three pupil regressors of interest per participant. The mean of these regressors was then correlated with the cartographic profile across all temporal windows for each of the 14 subjects (mean correlation, r = 0.241 ± 0.06). A set of one-sample t tests was then used to test whether the correlation between each bin of the cartographic profile was significantly different from zero (FDR α < 0.05). A similar t test was used to determine whether the correlation between the mean B_T and pupil diameter was significantly greater than zero across the cohort of 14 subjects.

Identifying Regions Related to Global Integration

We used a parcel-wise conjunction analysis (Nichols et al., 2005) to identify a set of regions in which the B_T and W_T were significantly related to drift rate, non-decision time, and pupil diameter. For each comparison in turn, we determined whether the W_T/B_T individual parcel was significantly correlated with each outcome measure of interest above chance (FDR α < 0.05). We then binarized the resultant parcel vectors and calculated a conjunction analysis separately for both W_T and B_T. Results were then projected onto surface renderings for interpretation.

Replication Analysis

To quantify how well our results replicated across sessions and datasets, we calculated group-level correlations between each of the measures identified in our analysis. Overall, we observed a strong positive correlation between the outcome measures identified in the two sessions (for all statistical tests, p < 0.001): graph measures, $-r_{W_T}$ = 0.982, r_{B_T} = 0.957; mean cartographic profiles, r_{Cart} = 0.982 (Figure S2). We also confirmed the presence of these results in a unique cohort of 92 unrelated participants from the HCP: graph measures, $- r_{W_T}$ = 0.971, r_{B_T} = 0.967; mean cartographic profiles, $- r_{Cart}$ = 0.973 (Figure S2). We also observed similarly positive relationships between the group-level outcome measures estimated from the HCP and NKI data (for all statistical tests, p < 0.001): graph measures, $- r_{W_T}$ = 0.941, r_{B_T} = 0.857; mean cartographic profiles, $- r_{Cart}$ = 0.927 (Figure S2). In addition, the same fluctuations observed in the HCP dataset were also present in the NKI dataset (see Video 3 at https://github.com/macshine/coupling).

Finally, the linear relationships between behavioral performance and the cartographic profile were consistent across the discovery and replication datasets. A spatial correlation between the two datasets was strongly positive for both the relationship with drift rate (r = 0.613; R^2 = 0.37; p = 10^{-11}; Figure S3) and non-decision time (r = 0.681; R^2 = 0.46; p = 10^{-15}; Figure S3), but the null hypothesis could not be rejected for the diffusion boundary (p > 0.500).

SUPPLEMENTAL INFORMATION

Supplemental Information includes Supplemental Experimental Procedures and four figures and can be found with this article online at http://dx.doi.org/10.1016/j.neuron.2016.09.018.

CellPress

AUTHOR CONTRIBUTIONS

ACKNOWLEDGMENTS

REFERENCES

Alavash, M., Thiel, C.M., and Gießing, C. (2016). Dynamic coupling of complex brain networks and dual-task behavior. Neuroimage 129, 233–246.

Aston-Jones, G., and Cohen, J.D. (2005). An integrative theory of locus coeruleus-norepinephrine function: adaptive gain and optimal performance. Annu. Rev. Neurosci. 28, 403–450.

Avants, B.B., Epstein, C.L., Grossman, M., and Gee, J.C. (2008). Symmetric diffeomorphic image registration with cross-correlation: evaluating automated labeling of elderly and neurodegenerative brain. Med. Image Anal. 12, 26–41.

Barch, D.M., Burgess, G.C., Harms, M.P., Petersen, S.E., Schlaggar, B.L., Corbetta, M., Glasser, M.F., Curtiss, S., Dixit, S., Feldt, C., et al.; WU-Minn HCP Consortium (2013). Function in the human connectome: task-fMRI and individual differences in behavior. Neuroimage 80, 169–189.

Bargmann, C.I., and Marder, E. (2013). From the connectome to brain function. Nat. Methods 10, 483–490.

Barttfeld, P., Uhrig, L., Sitt, J.D., Sigman, M., Jarraya, B., and Dehaene, S. (2015). Signature of consciousness in the dynamics of resting-state brain activity. Proc. Natl. Acad. Sci. USA 112, 887–892.

Bassett, D.S., Wymbs, N.F., Porter, M.A., Mucha, P.J., Carlson, J.M., and Grafton, S.T. (2011). Dynamic reconfiguration of human brain networks during learning. Proc. Natl. Acad. Sci. USA 108, 7641–7646.

Bassett, D.S., Yang, M., Wymbs, N.F., and Grafton, S.T. (2015). Learning-induced autonomy of sensorimotor systems. Nat. Neurosci. 18, 744–751.

Behzadi, Y., Restom, K., Liau, J., and Liu, T.T. (2007). A component based noise correction method (CompCor) for BOLD and perfusion based fMRI. Neuroimage 37, 90–101.

Betzel, R.F., Fukushima, M., He, Y., Zuo, X.-N., and Sporns, O. (2016). Dynamic fluctuations coincide with periods of high and low modularity in resting-state functional brain networks. Neuroimage 127, 287–297.

Bullmore, E., and Sporns, O. (2012). The economy of brain network organization. Nat. Rev. Neurosci. 13, 336–349.

Cole, M.W., Bassett, D.S., Power, J.D., Braver, T.S., and Petersen, S.E. (2014). Intrinsic and task-evoked network architectures of the human brain. Neuron 83, 238–251.

Cole, M.W., Yang, G.J., Murray, J.D., Repovš, G., and Anticevic, A. (2016). Functional connectivity change as shared signal dynamics. J. Neurosci. Methods 259, 22–39.

Corbetta, M., and Shulman, G.L. (2002). Control of goal-directed and stimulus-driven attention in the brain. Nat. Rev. Neurosci. 3, 201–215.

Deco, G., Tononi, G., Boly, M., and Kringelbach, M.L. (2015). Rethinking segregation and integration: contributions of whole-brain modelling. Nat. Rev. Neurosci. 16, 430–439.

Diedrichsen, J., Balsters, J.H., Flavell, J., Cussans, E., and Ramnani, N. (2009). A probabilistic MR atlas of the human cerebellum. Neuroimage 46, 39–46.

Duncan, J. (2010). The multiple-demand (MD) system of the primate brain: mental programs for intelligent behaviour. Trends Cogn. Sci. 14, 172–179.

Eldar, E., Cohen, J.D., and Niv, Y. (2013). The effects of neural gain on attention and learning. Nat. Neurosci. 16, 1146–1153.

Fries, P. (2015). Rhythms for cognition: communication through coherence. Neuron 88, 220–235.

Glasser, M.F., Sotiropoulos, S.N., Wilson, J.A., Coalson, T.S., Fischl, B., Andersson, J.L., Xu, J., Jbabdi, S., Webster, M., Polimeni, J.R., et al.; WU-Minn HCP Consortium (2013). The minimal preprocessing pipelines for the Human Connectome Project. Neuroimage 80, 105–124.

Godwin, D., Barry, R.L., and Marois, R. (2015). Breakdown of the brain's functional network modularity with awareness. Proc. Natl. Acad. Sci. USA 112, 3799–3804.

Gordon, E.M., Laumann, T.O., Adeyemo, B., Huckins, J.F., Kelley, W.M., and Petersen, S.E. (2016). Generation and evaluation of a cortical area parcellation from resting-state correlations. Cereb. Cortex 26, 288–303.

Guimerà, R., and Nunes Amaral, L.A. (2005). Functional cartography of complex metabolic networks. Nature 433, 895–900.

Hutchison, R.M., Womelsdorf, T., Gati, J.S., Everling, S., and Menon, R.S. (2013). Resting-state networks show dynamic functional connectivity in awake humans and anesthetized macaques. Hum. Brain Mapp. 34, 2154–2177.

Joshi, S., Li, Y., Kalwani, R.M., and Gold, J.I. (2016). Relationships between pupil diameter and neuronal activity in the locus coeruleus, colliculi, and cingulate cortex. Neuron 89, 221–234.

Kahneman, D. (1973). Attention and Effort (Experimental Psychology) (Prentice Hall).

Keller, C.J., Honey, C.J., Mégevand, P., Entz, L., Ulbert, I., and Mehta, A.D. (2014). Mapping human brain networks with cortico-cortical evoked potentials. Philos. Trans. R. Soc. Lond. B Biol. Sci. 369, 20130528.

Kitzbichler, M.G., Henson, R.N.A., Smith, M.L., Nathan, P.J., and Bullmore, E.T. (2011). Cognitive effort drives workspace configuration of human brain functional networks. J. Neurosci. 31, 8259–8270.

Krienen, F.M., Yeo, B.T.T., and Buckner, R.L. (2014). Reconfigurable task-dependent functional coupling modes cluster around a core functional architecture. Philos. Trans. R. Soc. Lond. B Biol. Sci. 369, http://dx.doi.org/10.1098/rstb.2013.0526.

Laumann, T.O., Gordon, E.M., Adeyemo, B., Snyder, A.Z., Joo, S.J., Chen, M.Y., Gilmore, A.W., McDermott, K.B., Nelson, S.M., Dosenbach, N.U., et al. (2015). Functional system and areal organization of a highly sampled individual human brain. Neuron 87, 657–670.

Mattar, M.G., Cole, M.W., Thompson-Schill, S.L., and Bassett, D.S. (2015). A functional cartography of cognitive systems. PLoS Comput. Biol. 11, e1004533.

McGinley, M.J., Vinck, M., Reimer, J., Batista-Brito, R., Zagha, E., Cadwell, C.R., Tolias, A.S., Cardin, J.A., and McCormick, D.A. (2015). Waking state: rapid variations modulate neural and behavioral responses. Neuron 87, 1143–1161.

Miyake, A., Friedman, N.P., Emerson, M.J., Witzki, A.H., Howerter, A., and Wager, T.D. (2000). The unity and diversity of executive functions and their contributions to complex "frontal lobe" tasks: a latent variable analysis. Cognit. Psychol. 41, 49–100.

Murphy, P.R., O'Connell, R.G., O'Sullivan, M., Robertson, I.H., and Balsters, J.H. (2014). Pupil diameter covaries with BOLD activity in human locus coeruleus. Hum. Brain Mapp. 35, 4140–4154.

CellPress

Murphy, P.R., van Moort, M.L., and Nieuwenhuis, S. (2016). The pupillary orienting response predicts adaptive behavioral adjustment after errors. PLoS ONE *11*, e0151763.

Nichols, T.E., and Holmes, A.P. (2002). Nonparametric permutation tests for functional neuroimaging: a primer with examples. Hum. Brain Mapp. *15*, 1–25.

Nichols, T., Brett, M., Andersson, J., Wager, T., and Poline, J.-B. (2005). Valid conjunction inference with the minimum statistic. Neuroimage *25*, 653–660.

Nooner, K.B., Colcombe, S.J., Tobe, R.H., Mennes, M., Benedict, M.M., Moreno, A.L., Panek, L.J., Brown, S., Zavitz, S.T., Li, Q., et al. (2012). The NKI-Rockland sample: a model for accelerating the pace of discovery science in psychiatry. Front. Neurosci. *6*, 152.

Pearlson, G.D., and Robinson, R.G. (1981). Suction lesions of the frontal cerebral cortex in the rat induce asymmetrical behavioral and catecholaminergic responses. Brain Res. *218*, 233–242.

Poldrack, R.A., Kittur, A., Kalar, D., Miller, E., Seppa, C., Gil, Y., Parker, D.S., Sabb, F.W., and Bilder, R.M. (2011). The cognitive atlas: toward a knowledge foundation for cognitive neuroscience. Front. Neuroinform. *5*, 17.

Power, J.D., Schlaggar, B.L., Lessov-Schlaggar, C.N., and Petersen, S.E. (2013). Evidence for hubs in human functional brain networks. Neuron *79*, 798–813.

Power, J.D., Mitra, A., Laumann, T.O., Snyder, A.Z., Schlaggar, B.L., and Petersen, S.E. (2014). Methods to detect, characterize, and remove motion artifact in resting state fMRI. Neuroimage *84*, 320–341.

Ramsey, J.D., Hanson, S.J., Hanson, C., Halchenko, Y.O., Poldrack, R.A., and Glymour, C. (2010). Six problems for causal inference from fMRI. Neuroimage *49*, 1545–1558.

Ratcliff, R. (1978). A theory of memory retrieval. Psychol. Rev. *85*, 59–108.

Ratcliff, R., Thompson, C.A., and McKoon, G. (2015). Modeling individual differences in response time and accuracy in numeracy. Cognition *137*, 115–136.

Rubinov, M., and Sporns, O. (2010). Complex network measures of brain connectivity: uses and interpretations. Neuroimage *52*, 1059–1069.

Safaai, H., Neves, R., Eschenko, O., Logothetis, N.K., and Panzeri, S. (2015). Modeling the effect of locus coeruleus firing on cortical state dynamics and single-trial sensory processing. Proc. Natl. Acad. Sci. USA *112*, 12834–12839.

Sara, S.J. (2009). The locus coeruleus and noradrenergic modulation of cognition. Nat. Rev. Neurosci. *10*, 211–223.

Shanahan, M. (2012). The brain's connective core and its role in animal cognition. Philos. Trans. R. Soc. Lond. B Biol. Sci. *367*, 2704–2714.

Shen, K., Hutchison, R.M., Bezgin, G., Everling, S., and McIntosh, A.R. (2015). Network structure shapes spontaneous functional connectivity dynamics. J. Neurosci. *35*, 5579–5588.

Shine, J.M., Koyejo, O., Bell, P.T., Gorgolewski, K.J., Gilat, M., and Poldrack, R.A. (2015). Estimation of dynamic functional connectivity using multiplication of temporal derivatives. Neuroimage *122*, 399–407.

Sigman, M., and Dehaene, S. (2008). Brain mechanisms of serial and parallel processing during dual-task performance. J. Neurosci. *28*, 7585–7598.

Smith, S.M., Beckmann, C.F., Andersson, J., Auerbach, E.J., Bijsterbosch, J., Douaud, G., Duff, E., Feinberg, D.A., Griffanti, L., Harms, M.P., et al.; WU-Minn HCP Consortium (2013). Resting-state fMRI in the Human Connectome Project. Neuroimage *80*, 144–168.

Sporns, O., and Betzel, R.F. (2016). Modular brain networks. Annu. Rev. Psychol. *67*, 613–640.

Steriade, M.M., and McCarley, R.W. (2013). Brainstem Control of Wakefulness and Sleep (Springer).

Tognoli, E., and Kelso, J.A. (2014). The metastable brain. Neuron *81*, 35–48.

van den Brink, R.L., Pfeffer, T., Warren, C.M., Murphy, P.R., Tona, K.-D., van der Wee, N.J.A., Giltay, E., van Noorden, M.S., Rombouts, S.A.R.B., Donner, T.H., and Nieuwenhuis, S. (2016). Catecholaminergic neuromodulation shapes intrinsic MRI functional connectivity in the human brain. J. Neurosci. *36*, 7865–7876.

van den Heuvel, M.P., and Sporns, O. (2013). Network hubs in the human brain. Trends Cogn. Sci. *17*, 683–696.

van den Heuvel, M.P., Bullmore, E.T., and Sporns, O. (2016). Comparative connectomics. Trends Cogn. Sci. *20*, 345–361.

Van der Werf, Y.D., Witter, M.P., and Groenewegen, H.J. (2002). The intralaminar and midline nuclei of the thalamus. Anatomical and functional evidence for participation in processes of arousal and awareness. Brain Res. Brain Res. Rev. *39*, 107–140.

van Ravenzwaaij, D., and Oberauer, K. (2009). How to use the diffusion model: parameter recovery of three methods: EZ, fast-dm, and DMAT. J. Math. Psychol. *53*, 463–473.

Varela, F., Lachaux, J.P., Rodriguez, E., and Martinerie, J. (2001). The brainweb: phase synchronization and large-scale integration. Nat. Rev. Neurosci. *2*, 229–239.

Vatansever, D., Menon, D.K., Manktelow, A.E., Sahakian, B.J., and Stamatakis, E.A. (2015). Default mode dynamics for global functional integration. J. Neurosci. *35*, 15254–15262.

Wagenmakers, E.-J., van der Maas, H.L.J., and Grasman, R.P.P.P. (2007). An EZ-diffusion model for response time and accuracy. Psychon. Bull. Rev. *14*, 3–22.

Yellin, D., Berkovich-Ohana, A., and Malach, R. (2015). Coupling between pupil fluctuations and resting-state fMRI uncovers a slow build-up of antagonistic responses in the human cortex. Neuroimage *106*, 414–427.

Zalesky, A., Fornito, A., Cocchi, L., Gollo, L.L., and Breakspear, M. (2014). Time-resolved resting-state brain networks. Proc. Natl. Acad. Sci. USA *111*, 10341–10346.